

Tune-out wavelengths and landscape modulated polarizabilities of alkali Rydberg atoms in infrared optical lattices

Turker Topcu and Andrei Derevianko

Department of Physics, University of Nevada, Reno, NV 89557, USA

(Dated: April 27, 2022)

Intensity modulated optical lattice potentials can change sign for an alkali metal Rydberg atom, and the atoms are not always attracted to intensity minima in optical lattices with wavelengths near the CO₂ laser band. Here we demonstrate that such IR lattices can be tuned so that the trapping potential seen by the Rydberg atom can be made to vanish for atoms in “targeted” Rydberg states. Such state selective trapping of Rydberg atoms can be useful in controlled cold Rydberg collisions, cooling Rydberg states, and species-selective trapping and transport of Rydberg atoms in optical lattices. We tabulate wavelengths at which the trapping potential vanishes for the ns , np , and nd Rydberg states of Na and Rb atoms, and discuss advantages of using such optical lattices for state selective trapping of Rydberg atoms. We also develop exact analytic expressions for the lattice induced polarizability for the $m_z = 0$ Rydberg states, and derive an accurate formula predicting tune-out wavelengths at which the optical trapping potential becomes invisible to Rydberg atoms in targeted $l = 0$ states.

PACS numbers: 37.10.Jk, 32.10.Dk, 32.80.Qk, 32.80.Rm

I. INTRODUCTION

Recent advances in quantum computing with Rydberg atoms, and quantum simulation experiments studying many-body systems have been possible thanks to developments in optical trapping methods [1–3]. Many of these experiments involve cold Rydberg atoms, such as implementations of quantum logical gates to realize scalable quantum computing [3, 4], and rely on optically trapped cold Rydberg atoms. Because of this, optical traps have been studied [5–9] as a method of trapping Rydberg atoms, alongside other trapping schemes involving static electric [10] and magnetic fields [11]. The main advantage of optical trapping stems from small dynamic Stark shifts experienced by the atomic states (MHz) compared to the shifts in electrostatic traps (GHz) [3].

Among various methods in optical trapping toolbox is the “tune-out” phenomena, where the optical lattice frequency is tuned to make it invisible to a once trapped atom. This method was first proposed by LeBlanc *et al.* [12], where an optical lattice is tuned to a wavelength at which the lattice potential vanishes for a given atomic species in ground state. This enables one to design species-specific optical lattices, where one atomic species is trapped and the other is “tuned out”. Such selectivity can be also achieved for different low-lying levels of the same atom, providing a state-specific optical lattice. These types of optical lattices have been investigated especially for ground state alkali metal atoms [13], and several applications have emerged over time, such as quantum computing schemes utilizing a storage lattice for encoding qubits and a transport lattice for addressing individual qubits [14], state-selective transport [15], and cooling in strongly correlated optical lattices [16].

The optical potential for off-resonant light vanishes for an atom in a specific state when its dynamic polarizability vanishes. This makes it straightforward to real-

ize species- and state-specific optical lattices for ground state atoms because the resonant structure at low-lying levels provides many frequencies at which the atomic polarizability vanishes. On the other hand, species-specific lattices have not been realized for Rydberg atoms, because the common wisdom is that the polarizability of a Rydberg state is essentially that of a free electron, which is always negative (although there has been evidence to the contrary [17]). Since the free electron polarizability does not change sign, it never vanishes, making it impossible to tune-out Rydberg atoms from optical lattices. In this paper, we demonstrate that this is not true, and tune-out wavelengths exist at which the optical lattice becomes invisible to a Rydberg atom in IR lattices with wavelengths up to $\sim 10^4$ nm. We tabulate a few of these tune-out wavelengths for some Rydberg states of Na and Rb atoms, and derive a simple analytical expression which accurately predicts half of the available tune-out wavelengths for alkali-metal atoms.

The trapping potential seen by the Rydberg electron is composed of an intensity modulated “landscaping” term and a constant offset, which does not depend on the position of the atom along the lattice [18]. This landscaping term modulates the free electron polarizability, and causes trapping potential to change sign. Because the trapping potential has to vanish in order to change sign, this allows us to tune out the lattice for Rydberg atoms in one state, while another state remains trapped.

In the next section, we provide a description of the tune-out phenomena for Rydberg atoms trapped in optical lattices. To this end, we use a one-dimensional toy model to introduce the underlying mechanism, and then proceed to rigorous treatment and calculation of the tune-out wavelengths for Na and Rb atoms. We then turn our attention to three-dimensional optical lattices in Sec. III. We evaluate intensity modulated polarizabilities in 3D lattices, and argue that tune-out can be achieved

for some states in all directions. Finally, we derive approximate analytic expressions for intensity modulated polarizabilities and tune-out wavelengths, which accurately predict half of the available tune-out wavelengths. We use atomic units throughout this paper unless we explicitly state otherwise.

II. TUNE-OUT FREQUENCIES FOR RYDBERG STATES

We start our description of the tune-out frequencies for Rydberg states using a toy model of a Rydberg atom in a one-dimensional optical lattice. In this model, the atom is one-dimensional and the electron density is concentrated on either side of the atom near the classical turning points at $z_e = \pm 2n^2$. This toy model of the Rydberg atom in a one-dimensional lattice is discussed in detail in [18], illustrating the interplay between the Rydberg orbit size and the lattice wavelength. Two cases when the size of the Rydberg orbit is larger and smaller than $\lambda/4$ correspond to cases in which the laser intensity maxima are the stable and unstable equilibrium points of the optical potential. As the wavelength of the lattice is varied from $\lambda/4 > 4n^2$ to $\lambda/4 < 4n^2$, there is the critical case when $\lambda/4 = 4n^2$ (Fig. 1). In this case, if the atom is displaced from the intensity maxima, one side falls inside the nearby inflection surface while the other falls outside. Because of the symmetry of the intensity distribution, the optical dipole forces \mathbf{f}_R and \mathbf{f}_L are equal in magnitude, and the atom feels no net tug, making it blind to the optical lattice. This is the “tune-out” situation we are interested in.

We will now derive explicit expressions for the dynamic polarizabilities of Rydberg states, which will allow us to calculate tune-out wavelengths for alkali-metal Rydberg atoms. The electric field of two linearly polarized counter-propagating laser beams can be used to construct a one-dimensional optical lattice:

$$\mathbf{F} = 2F_0\hat{\epsilon}\sin(\mathbf{k}\cdot\mathbf{r})\cos(\omega t), \quad (1)$$

where $k = \omega/c = 2\pi/\lambda$ is the wave vector, \mathbf{r} is the coordinate of the electron, F_0 is the electric field strength, and $\hat{\epsilon}$ is the polarization direction of the laser beams. We will work in the velocity gauge (also known as the transverse or the Coulomb gauge). In this gauge, the scalar potential is zero, and the vector potential \mathbf{A}_{VG} and the field are related by $\mathbf{F} = -\partial\mathbf{A}_{\text{VG}}/\partial t$. Then Hamiltonian for the electron is

$$H = \frac{p^2}{2} + V_C - \frac{\mathbf{A}_{\text{VG}}\cdot\mathbf{p}}{c} + \frac{(A_{\text{VG}})^2}{2c^2}, \quad (2)$$

where V_C is the core potential seen by the electron. The vector potential that gives rise to (1) in this gauge is

$$\mathbf{A}_{\text{VG}}(\mathbf{r}, t) = -\frac{2F_0}{\omega}\hat{\epsilon}\sin(\mathbf{k}\cdot\mathbf{r})\sin(\omega t). \quad (3)$$

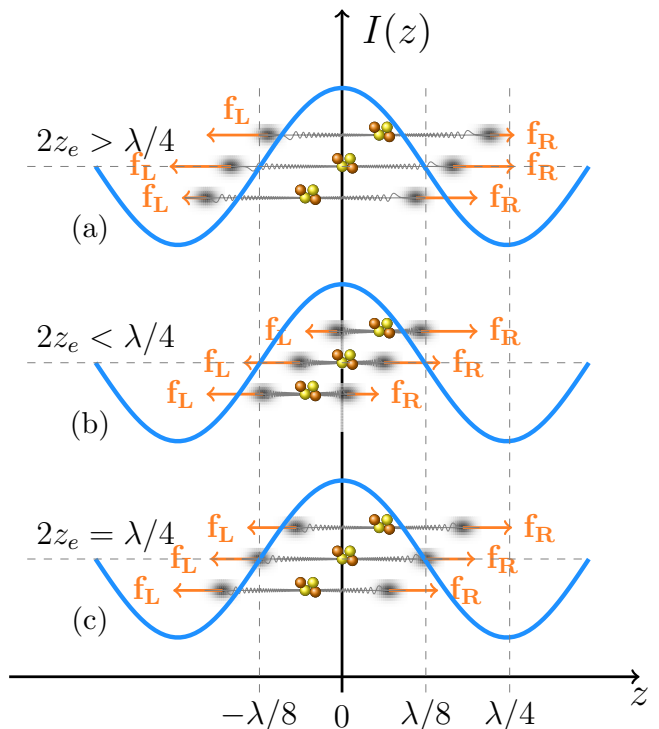


FIG. 1: Toy model of a Rydberg atom in one-dimensional lattice, where the vertical axis is the laser intensity $I(z)$. When the size of the Rydberg orbit $2z_e^0 = \lambda/4$, the forces \mathbf{f}_R and \mathbf{f}_L acting on the localized “lumps” of electron density are equal in magnitude and the net force acting on the atom is zero: this is the tune-out scenario.

Ref. [19] demonstrated that the last term in the Hamiltonian provides the dominant contribution to the energy shift for Rydberg states, which is what we will focus on. We use the first order perturbation theory for the $(A_{\text{VG}})^2$ term since it is already second order in the field strength. Then we can express the lattice potential for a Rydberg state $|r\rangle$ $U_r = -\alpha_r(\omega)F_0^2/4$, where $\alpha_r(\omega)$ is the dynamic polarizability for the Rydberg state $|r\rangle = |nlm_z\rangle$:

$$\alpha_{nlm_z}(\mathbf{R}, \omega) = -\frac{1}{\omega^2}\langle nlm_z|\sin^2(\mathbf{k}\cdot\mathbf{r})|nlm_z\rangle. \quad (4)$$

We can express the coordinate of the electron \mathbf{r} in terms of the center of mass coordinate of the atom \mathbf{R} and the coordinate of the Rydberg electron relative to the center of mass \mathbf{r}_e , *i.e.* $\mathbf{r} = \mathbf{r}_e + \mathbf{R}$. Since only the \mathbf{R} -dependent part of the lattice potential $U_r = -\alpha_r(\omega)F_0^2/4$ exerts force on the atom, it is advantageous to separate out the \mathbf{R} -dependent part of the polarizability, and refer to it as the trapping potential. Simple trigonometric manipulation leads to

$$\alpha_{nlm_z}(\omega) = -\frac{1}{\omega^2}\left[\sin^2(\mathbf{k}\cdot\mathbf{R})\langle nlm_z|\cos(2\mathbf{k}\cdot\mathbf{r}_e)|nlm_z\rangle + \langle nlm_z|\sin^2(\mathbf{k}\cdot\mathbf{r}_e)|nlm_z\rangle\right]. \quad (5)$$

At this point, we will assume a one-dimensional linearly polarized optical lattice propagating along the \hat{z} direction, so that $\mathbf{k} \cdot \mathbf{r}_e = kz_e$. We are also assuming that the energy splitting due to quantum defects between the low angular momentum states inside the n -manifold is much larger than the Stark coupling induced by the lattice field. In a one-dimensional lattice, this guarantees that the Rydberg atom stays in its initial state when trapped by the lattice field, since m is a good quantum number. In such a 1D lattice polarizability becomes

$$\alpha_{nlm_z}(\omega) = -\frac{1}{\omega^2} \left[\sin^2(kZ) \langle nlm_z | \cos(2kz_e) | nlm_z \rangle + \langle nlm_z | \sin^2(kz_e) | nlm_z \rangle \right], \quad (6)$$

where Z is the position of the atom along the z -axis. We can now separate the optical potential in two pieces:

$$U_r(Z) = U_r^0 + U_r^Z \sin^2(kZ), \quad (7)$$

where

$$U_r^Z = \frac{F_0^2}{4\omega^2} \langle nlm_z | \cos(2kz_e) | nlm_z \rangle \equiv -\alpha_{nlm_z}^{\text{isc}}(\omega) \frac{F_0^2}{4} \quad (8)$$

$$U_r^0 = \frac{F_0^2}{4\omega^2} \langle nlm_z | \sin^2(kz_e) | nlm_z \rangle. \quad (9)$$

The term U_r^0 is merely an ‘‘offset’’, and does not depend on where the atom is along the optical lattice. Therefore it exerts no force on the atom. It is the second term in (7) that is relevant in trapping the Rydberg atom. Here we introduced the intensity ‘‘landscape-averaged polarizability’’ $\alpha_{nlm_z}^{\text{isc}}(\omega)$, and unlike the free electron polarizability $\alpha_e = -1/\omega^2$, it can be both positive or negative depending on the wavelength. The fact that $\alpha_{nlm_z}^{\text{isc}}(\omega)$ can take both positive and negative values means that it has to vanish at certain wavelengths, and for these special λ the atom would be unaware of the optical lattice. This happens when

$$\alpha_{nlm_z}^{\text{isc}}(\omega) = -\frac{1}{\omega^2} \langle nlm_z | \cos(2kz_e) | nlm_z \rangle = 0, \quad (10)$$

which we refer to as the tune-out condition. The landscaping polarizability $\alpha_{nlm_z}^{\text{isc}}$ in this 1D lattice can be explicitly written by expanding $\cos(2kz_e)$ in spherical Bessel functions:

$$\begin{aligned} \alpha_{nlm_z}^{\text{isc}}(\omega) = & -\frac{(2l+1)}{\omega^2} \sum_{l'=\text{even}} (2l'+1)(-1)^{l'/2-m_z} \\ & \times \begin{pmatrix} l & l' & l \\ -m_z & 0 & m_z \end{pmatrix} \begin{pmatrix} l & l' & l \\ 0 & 0 & 0 \end{pmatrix} \quad (11) \\ & \times \int_0^\infty dr_e P_{nl}^2(r_e) j_{l'}(2kr_e). \end{aligned}$$

The Rydberg state landscaping polarizabilities $\alpha_{n,l,m_z}^{\text{isc}}(\omega)$ are calculated using non-relativistic states computed in a 12,000 a.u. radial box using 9000

points on a square-root mesh. We calculate $P_{nl}(r)$ by directly integrating the one-electron time-independent Schrödinger equation using the well known quantum defect potentials for the alkali atoms [20]. Finally, we plot $\alpha_{n,l,m_z}^{\text{isc}}$ to search for wavelengths at which the landscaping polarizability vanishes, and the optical lattice becomes invisible for the atom in state $|nlm_z\rangle$.

The matrix element $\langle nlm_z | \cos(2kz_e) | nlm_z \rangle$ in Eq. (10) can be seen as a factor modulating the free electron polarizability $\alpha_e = -1/\omega^2$ according to the intensity profile of the 1D lattice in the lattice propagation direction: $\alpha_{nlm_z}^{\text{isc}}(\omega) = \langle \cos(2kz_e) \rangle \alpha_e(\omega)$. We plot this modulation factor $\langle \cos(2kz_e) \rangle$ as a function of n for $l=0$ states of Rb atom in Fig. 2 for various wavelengths. In the upper panel, all curves start from 1 at small n , because in this limit $\langle \cos(2kz_e) \rangle \rightarrow 1$ and $\alpha_{nlm_z}^{\text{isc}}(\omega) \rightarrow \alpha_e(\omega)$. For larger n , they oscillate with diminishing amplitude towards higher n . Although oscillation amplitudes become smaller at larger n , they still go through $\langle \cos(2kz_e) \rangle = 0$, and each wavelength in the upper panel in Fig. 2 is a tune-out wavelength for an infinite number of ns -states with $n > 40$. Also note that the longer the wavelength the higher n it takes to modulate α_e .

The oscillations seen in the upper panel of Fig. 2 can be shown to harbor a universal character. For $l=0$ states, the modulation factor $\langle \cos(2kz_e) \rangle$ from Eq. (11) reduces to

$$\begin{aligned} \langle ns | j_0(2kr_e) | ns \rangle &= \langle ns | \sum_p c_p (kr_e)^p | ns \rangle \\ &= \sum_p c_p k^p \langle ns | r_e^p | ns \rangle, \quad (12) \end{aligned}$$

where we expanded $j_0(2kr_e)$ in power series. In the limit $n \rightarrow \infty$, we can use the expression $[\langle ns | r_e^p | ns \rangle]^{1/p} = b_p n^2$, where b_p is a coefficient. With this, we can show that

$$\begin{aligned} \langle j_0(2kr_e) \rangle &= \langle ns | \sum_p c_p b_p (kn^2)^p | ns \rangle \\ &= F(kn^2). \quad (13) \end{aligned}$$

In other words, the landscaping modulation factor $\langle \cos(2kr_e) \rangle$ is a function of kn^2 . The bottom panel of Fig. 2 illustrates this behavior where all the curves in upper panel are plotted as a function of $16n^2 a_0/\lambda$. The fact that all the curves lay on top of each other demonstrates the universal dependence on $k\langle r_e \rangle \propto n^2 a_0/\lambda$ for all wavelengths.

The actual landscaping polarizabilities $\alpha_{n,l,m_z}^{\text{isc}}(\omega)$ calculated using (11) for ns -states with $n=100$ (orange), 160 (black) and 180 (blue) for the Rb and Na atoms are plotted in Fig. 3. For all of these states, $\alpha_{ns}^{\text{isc}}(\omega)$ oscillates with increasing amplitude before dropping off like the free electron polarizability $\alpha_e = -1/\omega^2$ before $\lambda \sim 10^4$ nm. For all $\lambda < 10^4$ nm, there are infinitely many tune-out wavelengths for all Rydberg states before the oscillatory nature of $\alpha_{ns}^{\text{isc}}(\omega)$ is dominated by the free electron character. Table I tabulates the four largest

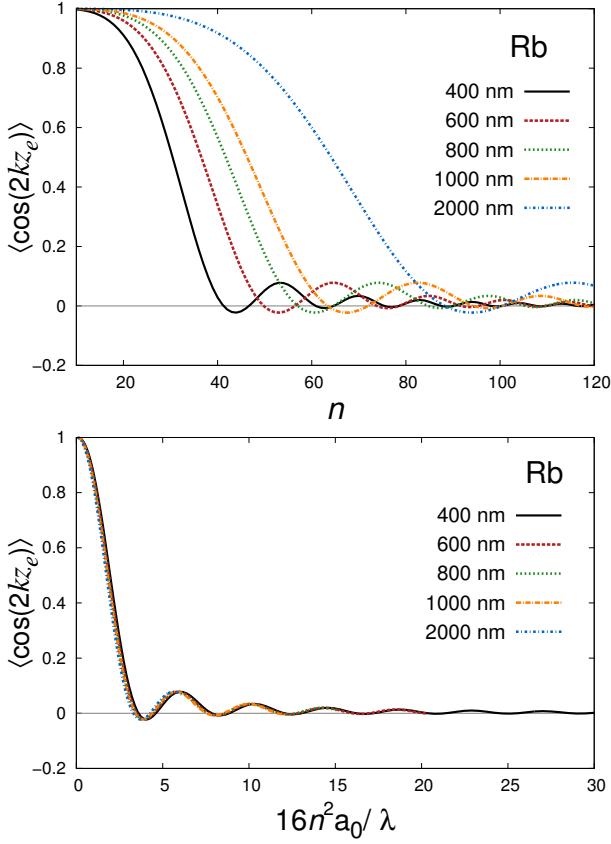


FIG. 2: The modulation factor $\langle \cos(2kz_e) \rangle$ as a function of n for $l = 0$ states of Rb for various λ . At low n , $\langle \cos(2kz_e) \rangle \rightarrow 1$ and $\alpha_{nlm_z}^{\text{isc}}(\omega) \rightarrow \alpha_e(\omega)$. At higher n , α_r^{isc} oscillates around zero, and each of the wavelengths seen in the figure becomes a tune-out wavelength for an infinite number of n states. The lower panel demonstrates the universal dependence of the factor $\langle \cos(2kz_e) \rangle$ from the upper panel on $n^2 a_0 / \lambda$.

tune-out wavelengths seen in Fig. 3. Furthermore, it includes the $n = 120$ s state and the p - and d -states in all of these n -manifolds for the Na and Rb atoms.

The behavior of $\alpha_{n,l,m_z}^{\text{isc}}(\omega)$ seen in Fig. 3 can be understood by realizing that $\cos(2kz_e) = 1 - 2\sin^2(kz_e)$, and

$$\alpha_{n,l,m_z}^{\text{isc}}(\omega) = -\frac{1}{\omega^2} (1 - 2\langle nlm_z | \sin^2(kz_e) | nlm_z \rangle). \quad (14)$$

For a given state, $\langle nlm_z | \sin^2(kz_e) | nlm_z \rangle \approx 1/2$ at small wavelengths and $\alpha_{n,l,m_z}^{\text{isc}} \approx 0$. As the wavelength is increased, kz_e gets smaller and $\langle nlm_z | \sin^2(kz_e) | nlm_z \rangle \ll 1$ resulting in the free electron polarizability dominating $\alpha_{n,l,m_z}^{\text{isc}}$. On the other hand, kz_e becomes larger at a given wavelength as n is increased, and $\alpha_{n,l,m_z}^{\text{isc}}$ oscillates until longer wavelengths before the free electron behavior takes over. All of these oscillations and crossings with the ground state polarizability occur at wavelengths in the CO₂ and the doubled CO₂ laser bands.

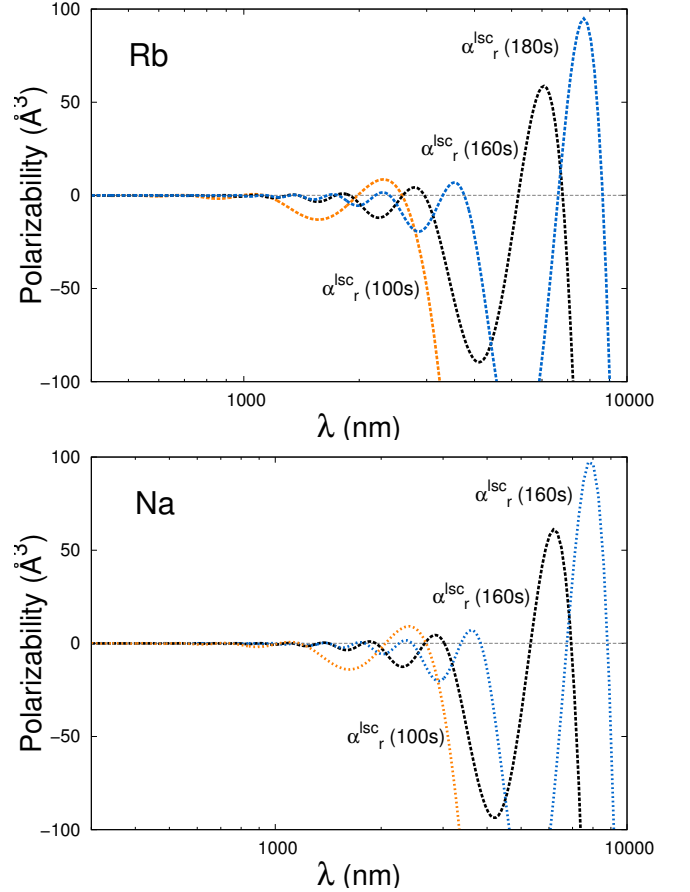


FIG. 3: Landscaping polarizabilities $\alpha_{n_s}^{\text{isc}}(\omega)$ for $n = 100, 160$ and 180 states of the Rb and Na atoms. The λ axis is plotted in logarithmic scale to display the range and amplitude of the oscillations. Note that $\sim 10^4$ nm is the center of the CO₂ laser band, and tune-out wavelengths can be found for all n in optical lattices with $\lambda < 10^4$ nm. Table I tabulates four largest tune-out wavelengths seen in this figure along with those for the p - and the d -states.

III. THREE-DIMENSIONAL OPTICAL LATTICES

So far we focused on one dimension. The position dependent polarizabilities in Fig. 3 are for the $l = 0$ Rydberg states, and exhibit tune-out frequencies in traps designed for one-dimensional confinement along the z -direction. If the 1D lattice is formed by counter-propagating Gaussian beams, the Rydberg atom may not be trapped in the radial direction. In this case, one could work with 3D lattices. Since the s -electron wave functions are spherically symmetric, the x , y , and z axes are equivalent, and our previous 1D arguments can be directly transferred to the 3D lattices. For the $l \neq 0$ states, 3D trapping may not be possible in all directions by proper choice of the lattice wavelength, as the quantization axis and three optical beam axes are no longer aligned [21]. In this case, the Rydberg atom

TABLE I: Four largest tune-out wavelengths (nm) for the s -, p - and the d -states in the $n = 100, 120, 160$ and 180 manifolds in Na and Rb atoms.

	100			120		
	s	p	d	s	p	d
Na	2688	4718	3909	3888	6813	5630
	2058	1825	2629	2978	2636	3787
	1171	1343	1323	1694	1939	1906
	1029	967	1063	1488	1396	1531
Rb	2589	4548	3805	3768	6608	5505
	1983	1759	2559	2887	2557	3702
	1128	1294	1288	1642	1881	1863
	991	932	1035	1443	1354	1497
	160			180		
	s	p	d	s	p	d
Na	6951	12156	10011	8814	15403	12670
	5324	4703	6732	6752	5959	8521
	3029	3460	3388	3841	4385	4288
	2662	2492	2722	3375	3157	3445
Rb	6790	11882	9843	8633	15095	12482
	5203	4597	6620	6614	5840	8394
	2959	3382	3332	3762	4297	4225
	2601	2436	2677	3307	3094	3394

may be trapped at an intensity maximum in one direction, while it may be trapped in intensity minima in other directions.

Formally the 3D lattice problem can be approached in the following fashion: First, we assume having six linearly polarized beams in three orthogonal directions. The polarization direction (E-field) defines the quantization axis. We then arrange two of the lattices (x and y axes would be the optical axes) to have the same polarization along the z -axis. If we add the third standing wave in the z -direction, its polarization will lay in the $x - y$ plane. If we choose the frequencies of the optical lattices to be slightly off, the interference effects can be made negligible [22]. Then we simply add the optical potentials independently: $U_{n,l,m_z}^R = U_{n,l,m_z}^X + U_{n,l,m_z}^Y + U_{n,l,m_z}^Z$,

$$U_{n,l,m_z}^X = -\alpha_{n,l,m_z}^{\text{lsc}}(\omega; X) \frac{F_0^2}{4}, \quad (15)$$

$$U_{n,l,m_z}^Y = -\alpha_{n,l,m_z}^{\text{lsc}}(\omega; Y) \frac{F_0^2}{4}, \quad (16)$$

$$U_{n,l,m_z}^Z = -\alpha_{n,l,m_z}^{\text{lsc}}(\omega; Z) \frac{F_0^2}{4}. \quad (17)$$

Here X, Y and Z refer to the lattice coordinates of the atom in the x, y and z directions. The associated land-

scaping polarizabilities are

$$\alpha_{n,l,m_z}^{\text{lsc}}(\omega_x; X) = -\frac{1}{\omega_x^2} \langle nlm_z | \cos(2k_x x) | nlm_z \rangle, \quad (18)$$

$$\alpha_{n,l,m_z}^{\text{lsc}}(\omega_y; Y) = -\frac{1}{\omega_y^2} \langle nlm_z | \cos(2k_y y) | nlm_z \rangle, \quad (19)$$

$$\alpha_{n,l,m_z}^{\text{lsc}}(\omega_z; Z) = -\frac{1}{\omega_z^2} \langle nlm_z | \cos(2k_z z) | nlm_z \rangle. \quad (20)$$

Because m_z is defined with respect to the z -axis, $\cos(2k_x x)$ and $\cos(2k_y y)$ will mix the degenerate m_z -states in a given l -manifold. However, as we discuss in Appendix A, this can be circumvented by either a proper choice of the laser frequency in the perpendicular directions, or by application of an external magnetic field.

We will pick the x -axis as the polarization axis of the third standing wave. Since the m_z -substates are defined with respect to the z -axis, the atom will be in a linear combination of m_x substates in the x -direction. To determine the optical potential in the z -direction, we need to find this linear combination, and then we can apply Eq. (11) since $\langle nlm_z | \cos(2kz) | nlm_z \rangle \equiv \langle nlm_x | \cos(2kx) | nlm_x \rangle$. For s -states all of this would not matter - *i.e.*, s -state Rydberg atoms exhibit oscillations seen in Fig. 3 and 2 no matter what. Also, in general one could pick the quantization axis (defined by external B-field) arbitrarily, and see if at some angle the polarizability can be made to vanish. We use the following procedure to evaluate the landscaping polarizabilities (18) in various (l, m_z)-states.

$$L_x(j, k) = \langle nlm_z | L_x | nlm'_z \rangle, \quad (21)$$

$$L_x(j, k) = \frac{1}{2} \left[\sqrt{(l - m'_z)(l + m'_z + 1)} \delta_{m_z, m'_z + 1} + \sqrt{(l - m'_z + 1)(l + m'_z)} \delta_{m_z, m'_z - 1} \right]. \quad (22)$$

Here we have labeled the states $|nlm_z\rangle$ and $|nlm'_z\rangle$ by j and k , and used

$$L_x = \frac{1}{2} (L_+ + L_-),$$

$$\langle l'm' | L_+ | lm \rangle = \sqrt{(l - m)(l + m + 1)} \delta_{l,l'} \delta_{m', m+1},$$

$$\langle l'm' | L_- | lm \rangle = \sqrt{(l - m + 1)(l + m)} \delta_{l,l'} \delta_{m', m-1}.$$

We then diagonalize the matrix L_x within the l -manifold of interest and obtain the eigenvalues and eigenvectors. The matrix $U_{j,\beta}$ whose columns are these eigenvectors is our rotation matrix in the Hilbert space:

$$\alpha_{n,l,m_z}^{\text{lsc}}(\omega; X) = -\frac{1}{\omega^2} \langle nlm_z | \cos(2kx) | nlm_z \rangle \quad (23)$$

$$= -\frac{1}{\omega^2} \sum_j d_{j,j} U_{j,\beta}^* U_{\beta,j}, \quad (24)$$

where we assumed $\omega_x = \omega_z \equiv \omega$, and β indexes the eigenstates of L_x within the l -manifold. In the end, $\alpha_{n,l,m_z}^{\text{lsc}}(\omega; X)$ is expressed as a linear combination of $\alpha_{n,l,m_z}^{\text{lsc}}(\omega; Z)$ within the same l -manifold. Here

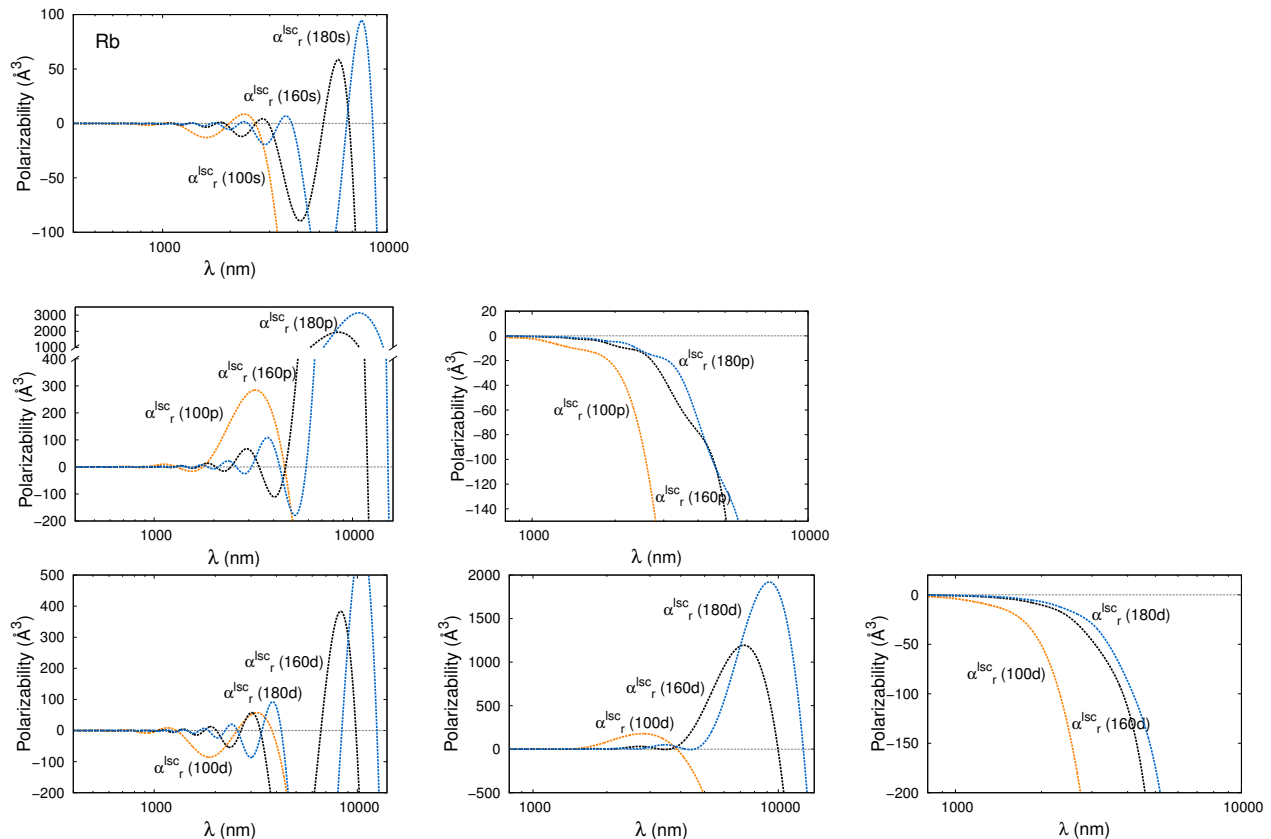
$m_z = 0$ $m_z = 1$ $m_z = 2$ 

FIG. 4: $\alpha_{n,l,m_z}^{\text{isc}}(\omega; Z)$ for l (rows) and m_z (columns) states for the Rb atom. Only $m_z > 0$ are shown since $\alpha_{n,l,m_z}^{\text{isc}}(\omega; Z)$ is identical for states with $+m_z$ and $-m_z$. For $(l, m_z) = (0,0)$, $(1,0)$, $(2,0)$, and $(2,1)$ $\alpha_{n,l,m_z}^{\text{isc}}(\omega; Z)$ oscillates and the angular coefficients in (11) come in with different signs. For the $(1,1)$ and $(2,2)$ states, it is always negative because the angular coefficients in (11) are all positive.

we are exploiting the identity $\langle nlm_z | \cos(2kz) | nlm_z \rangle \equiv \langle nlm_x | \cos(2kx) | nlm_x \rangle$ between the matrix elements,

which can be evaluated using Eq. (11).

Landscaping polarizabilities $\alpha_{n,l,m_z}^{\text{isc}}(\omega; Z)$ for a one-dimensional optical lattice with polarization in the z -direction are seen in Fig. 4 when the Rydberg atom is in s -, p - and d -states. The rows in the figure represent $l = 0, 1$ and 2 from top to bottom, and the columns are the m_z substates. Because Eq. (11) is identical for $\pm|m_z|$ states within the same l -manifold, we only plot $m_z > 0$ states in Fig. 4. For all $m_z = 0$ states, the landscaping polarizability oscillates and the atom is trapped at intensity minima when $\alpha_{n,l,0}^{\text{isc}}(\omega; Z) < 0$ and it is trapped at intensity maxima when $\alpha_{n,l,0}^{\text{isc}}(\omega; Z) > 0$. As the wavelength varies, there are wavelengths at which this high and low intensity seeking character turns into one another. At these wavelengths, $\alpha_{n,l,0}^{\text{isc}}(\omega; Z)$ vanishes and the optical lattice is invisible to the atom. On the other

hand, such tune-out wavelengths only exist for p -states when $m_z = 1$, and they are non-existent for the extreme m_z states for $l > 0$. In these circular states, the landscaping polarizability is always negative, and the atom always seeks low intensity and is aware of the trapping potential.

We now turn on a second lattice with perpendicular polarization to the first one. We take the polarization of this second beam to be in the x -direction. Then the landscaping polarizabilities for the same Rydberg states in Fig. 4 are seen in Fig. 5. In this case, states with $m_z = \pm|l|$ exhibit tune-out conditions for all l , and the $m_z = 0$ states for $l > 0$ behave as the circular states in Fig. 4. There are no tune-out wavelengths for these states and the atom is always attracted to intensity minima.

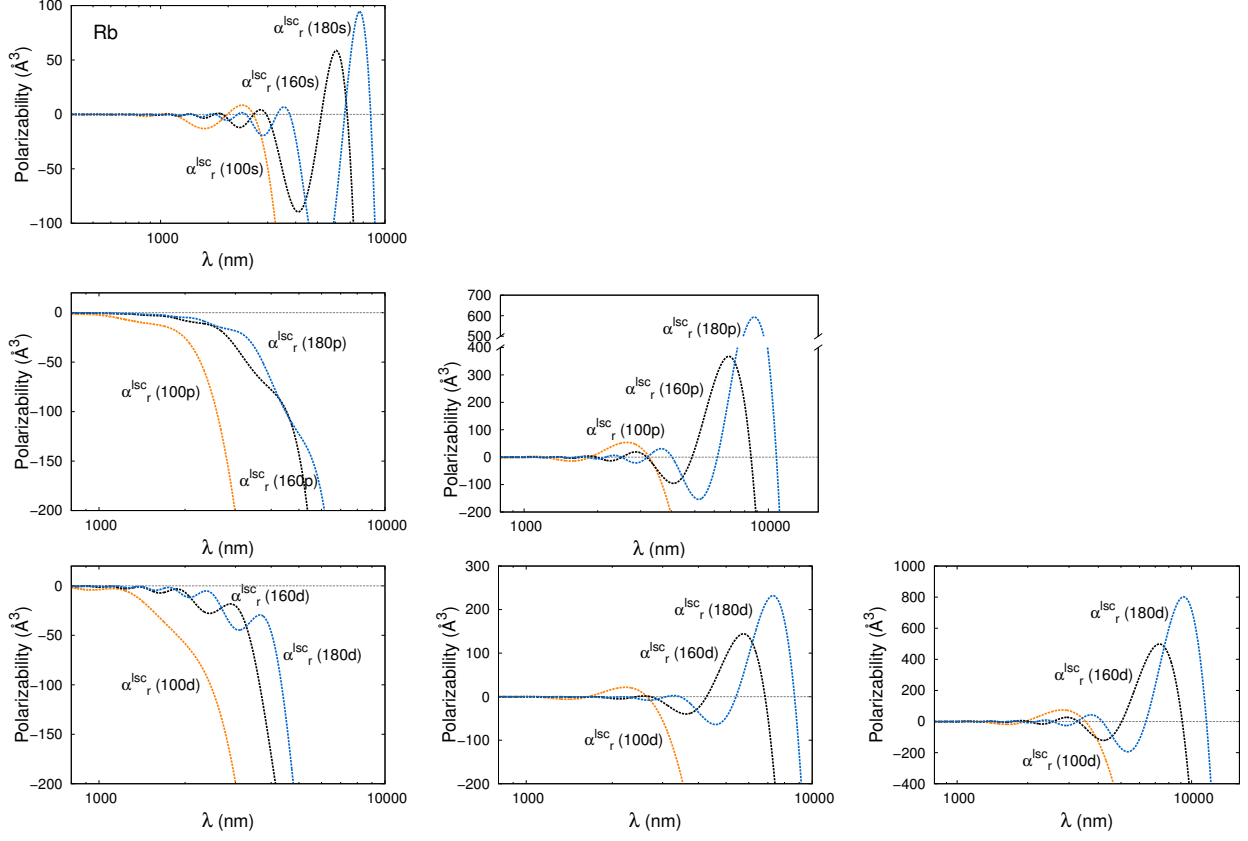
$m_z = 0$ $m_z = 1$ $m_z = 2$ 

FIG. 5: $\alpha_{n,l,m_z}^{\text{isc}}(\omega; X)$ for l (rows), m_z (columns) states for the Rb atom. Only $m_z > 0$ are shown because $\alpha_{n,l,m_z}^{\text{isc}}(\omega; X)$ is a linear combination of $\alpha_{n,l,m_z}^{\text{isc}}(\omega; Z)$ within the l -manifold when z is chosen to be the quantization axis, and $\alpha_{n,l,m_z}^{\text{isc}}(\omega; Z)$ are identical for states with $+m_z$ and $-m_z$ from Eq. (11). Note that $\alpha_{n,l,m_z}^{\text{isc}}(\omega; X)$ and $\alpha_{n,l,m_z}^{\text{isc}}(\omega; Z)$ are the same for $l = 0$.

IV. ANALYTICAL EXPRESSIONS FOR TUNE-OUT WAVELENGTHS

For individual l -states, closed form analytical expressions can be derived for Eq. (20) using hydrogenic radial wave functions, and the results can be generalized for alkali atoms by changing principal quantum number n to effective n^* and changing orbital angular momentum l to effective l^* (to keep the number of radial nodes fixed). We will start with the expression for the landscaping part of the Rydberg state polarizability for the case of linearly polarized laser beams where z -axis is the propagation axis:

$$\alpha_{n,l,m_z}^{\text{isc}}(k) = -\frac{1}{\omega^2} \langle nlm_z | \cos(2kz_e) | nlm_z \rangle, \quad (25)$$

and $k = 2\pi/\lambda$ is the wavevector. The matrix element in (25) can be expressed as an expansion in the spherical Bessel functions $j_\nu(r_e)$ as in Eq.(11) for given state $|nlm_z\rangle$. Specifically, for $l = 0, 1$ and 2 , and $m_z = 0$, the

landscaping polarizability $\alpha_{n,l,m_z}^{\text{isc}}$ can be expressed as

$$\begin{aligned} \alpha_{n,0,0}^{\text{isc}}(k) &= -\frac{1}{\omega^2} \int_0^\infty dr_e P_{n,0}^2(r_e) j_0(2kr_e), \\ \alpha_{n,1,0}^{\text{isc}}(k) &= -\frac{1}{\omega^2} \int_0^\infty dr_e P_{n,1}^2(r_e) [j_0(2kr_e) - 2j_2(2kr_e)], \\ \alpha_{n,2,0}^{\text{isc}}(k) &= -\frac{1}{\omega^2} \int_0^\infty dr_e P_{n,2}^2(r_e) [j_0(2kr_e) - \frac{10}{7}j_2(2kr_e) \\ &\quad + \frac{18}{7}j_4(2kr_e)]. \end{aligned}$$

These expressions can be represented with the aid of the definition,

$$s_{n,l,q}(k) \equiv -\frac{1}{\omega^2} \int_0^\infty dr_e P_{n,l}^2(r_e) j_q(2kr_e), \quad (26)$$

so that the above expressions for the landscaping polarizabilities read :

$$\alpha_{n,0,0}^{\text{isc}}(k) = s_{n,0,0}(k), \quad (27)$$

$$\alpha_{n,1,0}^{\text{isc}}(k) = s_{n,1,0}(k) - 2s_{n,1,2}(k), \quad (28)$$

$$\alpha_{n,2,0}^{\text{isc}}(k) = s_{n,2,0}(k) - \frac{10}{7}s_{n,2,2}(k) + \frac{18}{7}s_{n,2,4}(k) \quad (29)$$

We derive closed form expressions for $s_{n,l,q}$ in Appendix B using the well known radial wave functions for the hydrogen atom.

A. Landscaping polarizabilities and tune-out wavelengths for s -states

Since $l = 0$ is the simplest case (Eq. (27)), we would like to obtain an approximate expression for $\alpha_{n,0}^{\text{isc}}$ and the tune-out wavelengths at which it vanishes. For an s -state, $\alpha_{n,0}^{\text{isc}} = s_{n,0,0}$ and therefore $q = 0$. In our derivation, we will only keep the leading term in the sum (44). This will undermine the oscillatory character of the Rydberg state and we find that it yields an accurate expression for half of the tune-out frequencies. The reason that ignoring the oscillations of the Rydberg orbital yields us anything acceptable is that the main contribution to the integral in (11) comes from near the classical turning point, where the oscillatory parabolic nature of the Rydberg orbital assumes an exponentially decaying hyperbolic form. By only taking the largest order term in the Laguerre polynomials, we are still ensuring that this part of the wavefunction is included in our approximate Rydberg orbital, albeit with overestimated amplitude. Thus, keeping the leading term in the sum (44), we obtain

$$\alpha_{n,0}^{\text{isc}} \simeq -A_{n^*l^*} \frac{(1 + \xi^2)^{-n^*}}{\xi^3} \sin[2n^* \tan^{-1} \xi], \quad (30)$$

where $A_{n^*l^*}$ is a coefficient. This expression vanishes when the argument of the sine function is an integer multiple of π , meaning that the atom will not feel the optical lattice when

$$2n^* \tan^{-1} \xi^\otimes = p\pi \quad (p = 1, 2, \dots) \\ \xi^\otimes = k^\otimes n^* = \left| \tan\left(\frac{p\pi}{2n^*}\right) \right|. \quad (31)$$

The index p counting the roots start from 1 because $p = 0$ results in infinitely long wavelength. In increasing order, p yields half of the available tune-out wavelengths from longer to shorter wavelengths. Thereby the tune-out wavelengths are

$$\lambda_p^\otimes = \frac{2\pi n^*}{\tan[p\pi/(2n^*)]}. \quad (32)$$

For large n^* (or small values of $p\pi/(2n^*)$), this has the scaling $\lambda_p^\otimes \sim 4(n^*)^2/p$.

TABLE II: Calculated λ^\otimes versus the analytically estimated λ_p^\otimes (nm) from Eq. (32) for 160s and 180s states of Na and Rb. $n = 160$ refers to $n^* = 158.58$ and 156.76 , and $n = 180$ refers to $n^* = 178.58$ and 176.75 for Na and Rb, respectively.

	160		180	
	λ^\otimes	λ_p^\otimes	λ^\otimes	λ_p^\otimes
Na	6951		8814	
	<u>5324</u>	<u>5323</u>	<u>6752</u>	<u>6750</u>
	3029		3841	
	<u>2662</u>	<u>2661</u>	<u>3375</u>	<u>3375</u>
Rb	6790		8633	
	<u>5203</u>	<u>5201</u>	<u>6614</u>	<u>6613</u>
	2959		3762	
	<u>2601</u>	<u>2600</u>	<u>3307</u>	<u>3306</u>

In Table II, we present a comparison of the analytical and the numerically evaluated λ^\otimes . The tune-out wavelengths predicted by (32) are tabulated in Table II together with the exact values for 160s and 180s states of Na and Rb. Note that our analytical expression only predicts every other available tune-out wavelength, although it is a very good approximation for the ones it can predict. The agreement for these λ^\otimes is better than a part in a thousand for both Na and Rb atoms. Although taking only the leading term in the Laguerre polynomial to approximate the radial part of the integral in (11) is a very crude approximation (because it ignores the oscillatory nature of the Rydberg wavefunction), this approximation predicts half of the tune-out wavelengths surprisingly well.

V. CONCLUSIONS

Many recent advances in precision time keeping, quantum control with cold molecules and quantum computation science rely on trapping cold atoms and molecules in optical lattices. The common wisdom is that alkali atoms in Rydberg states see trapping potentials that are essentially that of a free electron, and are always low intensity seekers in an optical lattice. The change in the high and low intensity seeking character of the Rydberg states results from a non-monotonic interplay between the lattice constant and the physical size of the Rydberg state. Recently, we demonstrated that this view needs revision, and Rydberg atoms can be made to be both low and high intensity seekers by proper choice of lattice wavelength [18]. In other words, the lattice potential can be positive or negative for a given Rydberg state. To change sign, the lattice potential has to vanish at certain wavelengths at which the optical lattice becomes invisible to the atom. In this paper, we have illustrated this phe-

nomenon through extensive calculations. At these frequencies, the atom in the targeted state is “tuned out” of the lattice, while atoms in other Rydberg states are still trapped at either intensity minima or maxima. We have provided a list of these tune-out wavelengths for a few highly excited states of alkali metal atoms Na and Rb in one-dimensional IR lattices.

We then turn our attention to optical lattices beyond one-dimension, and demonstrate that the optical lattice potential does not change sign for all Rydberg states $|nlm_z\rangle$ for a given lattice polarization by simply tuning the lattice wavelength. For example, for a one-dimensional lattice formed by two laser beams propagating along the z -axis with polarization in the x -direction, the landscaping polarizability exhibits tune out wavelengths only for the $m_z = 0$ states and the $m_z = \pm 1$ states for $l = 2$. The optical potential does not change sign for any of the circular states with $l > 1$. In contrast, when we turn on a second standing wave propagating along the x -axis with polarization in the z -direction, only the $l = 0$ and the extreme $|m_z|$ states exhibit tune-out wavelengths. In this two-dimensional setup, tune-out wavelengths exist simultaneously in both lattices only for the s -states and d -states with $m_z = \pm 1$.

We also derive closed form analytic expressions for the tune-out wavelengths of alkali metal atoms in $m_z = 0$ Rydberg states trapped in IR optical lattices. Using these expressions, we obtain a simple formula for s -states, which accurately predicts half of the available tune-out wavelengths.

VI. ACKNOWLEDGMENTS

This work was supported by the National Science Foundation (NSF) Grant No. PHY-1212482 and PHY05-25915.

VII. APPENDIX A

Here we demonstrate that in the presence of a second standing wave with polarization perpendicular to the z -direction, the mixing between different degenerate m_z sublevels in a Ry l -manifold can be prevented by a proper choice of the laser frequency. This is particularly useful when there are no tune-out conditions in the second direction, and the lattice wavelength can be chosen freely without the tune-out constraint. This situation occurs in Fig. 5 for several m_z -states. When the tune-out condition also needs to be achieved in the second direction, an external magnetic field can be applied to split the m_z sublevels so that the splitting is much larger than the matrix elements connecting different m_z states. This would effectively prevent m_z mixing inside a Ry l -manifold. In this section, we will assume that the second standing wave is polarized in the x -direction.

Because $\sin(2kx_e)$ mixes different m_z substates, it is necessary to construct and diagonalize the matrix

$$\mathbf{U}_r^X = -\frac{F_0^2}{4}\boldsymbol{\alpha}(\omega; X), \quad (33)$$

to obtain the optical potential in the second direction. Here $\boldsymbol{\alpha}(\omega; X)$ is the landscaping polarizability matrix, and the matrix elements of \mathbf{U}_r^X and $\boldsymbol{\alpha}(\omega; X)$ are

$$U_r^X(nlm_z; n'l'm'_z) = -\frac{F_0^2}{4}\alpha_{n,l,m}^{n',l',m'}(\omega; X), \quad (34)$$

$$\alpha_{n,l,m}^{n',l',m'}(\omega; X) \equiv -\frac{1}{\omega^2}\langle nlm|\cos(2kx_e)|n'l'm'\rangle. \quad (35)$$

For example, \mathbf{U}_r^X is a 3×3 matrix for a p -state where only the diagonal and $U_r^X(n, 1, \pm 1; n, 1, \mp 1)$ off-diagonal matrix elements are non-zero.

The operator we have been using to evaluate the landscaping polarizability in the z -direction is

$$\begin{aligned} \cos(2kz_e) &= \sum_{L=\text{even}} (2L+1)(-1)^{L/2} j_L(2kr_e) P_L(\cos\theta) \\ &= \sum_{L=\text{even}} a_{L,0}(r) Y_{L,0}(\hat{r}), \end{aligned} \quad (36)$$

where $a_{L,0}(r) = (-1)^{L/2} \sqrt{4\pi(2L+1)} j_L(2kr_e)$, j_L are spherical Bessel functions, and $Y_{L,M}$ are the spherical harmonics. We would like to rotate z_e into x_e such that $\cos(2kz_e) \rightarrow \cos(2kx_e)$, where \hat{S} is an operator that rotates z_e to x_e . The effect of rotation on the spherical harmonics can be expressed in terms of the Wigner D-functions [23]:

$$Y_{L,M'}(\hat{S}\hat{r}) = \sum_{M=-L}^L Y_{L,M}(\hat{r}) D_{MM'}^L(\alpha, \beta, \gamma), \quad (37)$$

where (α, β, γ) are the Euler angles. With the choice of angles $(0, \pi/2, 0)$, the operator $\cos(2kx_e)$ can be written as

$$\begin{aligned} \cos(2kx_e) &= \sum_{L,M} a_{L,0}(r) Y_{L,M}(\hat{S}\hat{r}) \\ &= \sum_{L,M} a_{L,0}(r) Y_{L,M}(\hat{r}) D_{M0}^L(0, \pi/2, 0), \end{aligned}$$

where L is even. From Ref. [23]

$$D_{M0}^L(\alpha, \beta, \gamma) = \sqrt{\frac{4\pi}{2L+1}} Y_{LM}^*(\beta, \alpha), \quad (38)$$

which leads to

$$\cos(2kx_e) = \sum_{L,M} T_M^{(L)} \sqrt{\frac{4\pi}{2L+1}} Y_{LM}^*(\pi/2, 0). \quad (39)$$

Here we have defined $T_M^{(L)} \equiv a_{L,0}(r) Y_{L,M}(\hat{r})$. The matrix elements of $\boldsymbol{\alpha}(\omega; X)$ therefore become

$$\alpha_{n,l,m}^{n',l',m'}(\omega; X) \equiv -\frac{1}{\omega^2} \sum_{L,M} B_{L,M} \langle nlm|T_M^{(L)}|n'l'm'\rangle. \quad (40)$$

For the specific Euler angles $\beta = \pi/2$ and $\alpha = 0$, a closed form expression can be found for $Y_{LM}^*(\pi/2, 0)$ [23], and the coefficients $B_{L,M}$ become

$$B_{L,M} = \begin{cases} (-1)^{\frac{L+M}{2}} \sqrt{\frac{(L+M-1)!! (L-M-1)!!}{(L+M)!! (L-M)!!}} & L+M \text{ even} \\ 0 & L+M \text{ odd} \end{cases}$$

Using the Wigner-Eckart theorem, we can express the matrix elements for the operator $T_M^{(L)}$ in terms of the reduced matrix elements:

$$\langle nlm_z | T_M^{(L)} | n'l'm'_z \rangle = (-1)^{l-m_z} \times \begin{pmatrix} l & L & l' \\ -m_z & M & m'_z \end{pmatrix} \langle nl || T^{(L)} || n'l' \rangle, \quad (41)$$

where

$$\langle nl || T^{(L)} || n'l' \rangle = (2L+1)(-1)^{\frac{L}{2}-l} \sqrt{(2l+1)(2l'+1)} \times \begin{pmatrix} l & L & l' \\ 0 & 0 & 0 \end{pmatrix} \int_0^\infty dr_e P_{nl}(r_e) j_L(2kr_e) P_{n'l'}(r_e).$$

This method of evaluating the landscaping polarizabilities $\alpha_{n,l,m}^{\text{isc}}(\omega; X)$ reproduces Fig. 5, which was calculated by rotating the eigenstates. The diagonal matrix elements of $\alpha(\omega; X)$ correspond to $\alpha_{n,l,m}^{\text{isc}}(\omega; X)$.

Evaluating the diagonal and off-diagonal matrix elements of the landscaping polarizability matrix $\alpha(\omega; X)$, we see that the off-diagonal matrix elements can be comparable to the diagonal elements at certain wavelengths. On the other hand, the off-diagonal matrix elements can be also made to vanish at several wavelengths. For example, in Fig. 6 we plot the $m_z = 0$ diagonal matrix element and the only non-zero off-diagonal element for the 100p state of Rb. This diagonal matrix elements is identical to the landscaping polarizability seen in the second row of Fig. 5 for $m_z = 0$. It is also clear that the diagonal matrix element vanishes at several wavelengths, such as 1642, 1401, 897, and 815 nm. At these wavelengths $\alpha(\omega; X)$ is diagonal, therefore there is no mixing between the different m_z -states of the 100p manifold.

Alternatively, one can apply an external magnetic field B to lift the degeneracy between m_z states such that the Zeeman splitting is much larger than the off-diagonal matrix elements. In this case, the splitting occurs only between the diagonal matrix elements, and the optical potential becomes $\mathbf{U}_r^X + m\mu_B B \mathbf{I}$, where μ_B is the magnetic moment and \mathbf{I} is the identity matrix. This means that when magnetic field is chosen so that $\mu_B B \gg U_r^X(n, 1, \pm 1; n, 1, \mp 1)$, where $U_r^X(n, 1, \pm 1; n, 1, \mp 1)$ is comparable to the diagonal matrix elements, the optical potential can be made essentially diagonal, effectively preventing mixing between the

m_z sublevels of the l -manifold. For example, for a Ry state in a 10 mK deep optical trap, the external magnetic field needed to split the degenerate levels by 10 mK is ~ 150 Gauss. Similar considerations apply for an optical lattice oriented in the y -direction.

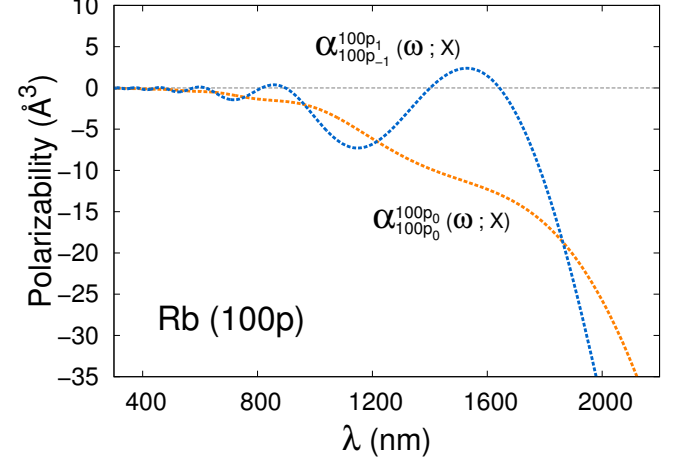


FIG. 6: (Color online) Diagonal $\alpha_{100p_0}^{100p_0}(\omega; X)$ (dashed orange) and off-diagonal $\alpha_{100p_{-1}}^{100p_1}(\omega; X)$ (dashed blue) matrix elements of the landscaping polarizability matrix $\alpha(\omega; X)$. The off-diagonal matrix element vanishes at several wavelengths.

VIII. APPENDIX B

In order to derive closed form analytical expressions for $s_{n,l,q}$ defined in Sec. IV, we use the well known radial wave functions for the hydrogen atom in terms of the associated Laguerre polynomials [20]:

$$R_{n,l}(r_e) = \frac{2}{n^2} \sqrt{\frac{(n-l-1)!}{(n+l)!}} \left(\frac{2r_e}{n}\right)^l e^{-r_e/n} L_{n-l-1}^{2l+1}\left(\frac{2r_e}{n}\right).$$

Then by substituting this into Eq. (26) and defining $\xi = kn$, $\rho = 2r_e/n$ and simplifying, we get

$$s_{nl}(\xi) = -\frac{n^2 (n-l-1)!}{c^2 \xi^2 2n (n+l)!} \times \int_0^\infty e^\rho \rho^{2(l+1)} [L_{n-l-1}^{2l+1}(\rho)]^2 j_q(\xi \rho) d\rho, \quad (42)$$

where $[L_{n-l-1}^{2l+1}(\rho)]^2$ is the square of the Laguerre polynomial [24]:

$$[L_{n_r}^\alpha(\rho)]^2 = \frac{(n_r + \alpha)!}{2^{2n_r} n_r!} \sum_{j=0}^{n_r} \frac{(2j)! (2n_r - 2j)!}{j! \{(n_r - j)!\}^2 (\alpha + j)!} \sum_{k=0}^{2j} \frac{(2j + 2\alpha)! 2^k}{(2j - k)! (2\alpha + k)!} \frac{(-1)^k}{k!} \rho^k \quad (43)$$

with $n_r = n - l - 1$ (number of radial nodes) and $\alpha = 2l + 1$. Eqs. (42) and (43) can be used to cast $s_{nl}(\xi)$ into a finite sum of the form

$$s_{n,l,q}(\xi) = \frac{1}{k^3} \sum_{p=0}^{2n_r} b_p I_p(q), \quad (44)$$

where $I_p(q)$ involves the integrals over ρ , and b_p are coefficients involving quantum numbers. We now derive

coefficients b_p and the integrals $I_p(q)$.

Expression (43) is a nested double sum, where the power of ρ is k , the index of the *inner* sum. Therefore, Eq. (43) gives a polynomial in a form which has more than one term involving a given power of ρ . To obtain the coefficients b_j , we need an expression in which the powers of ρ are in terms of the index of the *outer* summation. This can be done by rearranging the terms in Eq. (43) in the following fashion:

$$[L_{n_r}^\alpha(\rho)]^2 = \frac{(n_r + \alpha)!}{2^{2n_r} n_r!} \sum_{p=0}^{2n_r} \sum_{g=0}^{G(p)} \frac{(2n_r - 2g)! (2g)!}{(n_r - g)! \{g!\}^2 (\alpha + n_r - g)!} \times \frac{(2n_r - 2g + 2\alpha)! 2^{2n_r - p}}{(p - 2g)! (2\alpha + 2n_r - p)! (2n_r - p)!} \rho^{2n_r - p}, \quad (45)$$

$$G(p) = \frac{1}{2} \left[p - \frac{1}{2} (1 - (-1)^p) \right]. \quad (46)$$

Notice that $G(p)$ is the upper limit of the inner sum in Eq. (45). Although these expressions are for the hydrogen atom, they can be generalized to the case of an alkali atom utilizing the quantum defect theory such that the energy of a given state in an alkali atom fits the hydrogenic form $-1/[2(n^*)^2]$ [20], and the number of radial nodes $n_r = n - l - 1 = n^* - l^* - 1$ is fixed [25]. This pro-

duces a new set of quantum numbers (n^* and l^*) for the alkali atom, and since they are no longer integers, the factorials in (45) must be expressed in terms of the Gamma function when necessary, *i.e.*, $\Gamma(x) = (x - 1)!$. Following through this procedure and using the rearranged version of the squared Laguerre polynomials given by Eq. (45), $s_{n,l,q}$ can be written as

$$s_{n,l,q}(\xi) = \frac{n^*}{2c^2 \xi^3} \frac{1}{2^{2n_r}} \sum_{p=0}^{2n_r} \left(\sum_{g=0}^{G(p)} \frac{\Gamma(2n_r - 2g + 1) (2g)!}{\Gamma(n_r - g + 1) \{g!\}^2 \Gamma(\alpha^* + n_r - g + 1)} \right) \times \frac{\Gamma(2n_r - 2g + 2\alpha^* + 1) 2^{2n_r - p}}{(p - 2g)! \Gamma(2\alpha^* + 2n_r - p + 1) \Gamma(2n_r - p + 1)} \frac{(-1)^{2n_r - p}}{\Gamma(2n_r - p + 1)} \times \underbrace{\int_0^\infty e^{-\rho} \rho^{2n^* - p} j_q(\xi \rho) d\rho}_{I_p(q)}.$$

On identifying with Eq. (44), we find

$$\begin{aligned}
 n_r &= n - l - 1 = n^* - l^* - 1 \quad \text{and} \quad \alpha^* = 2l^* + 1, \\
 b_p &= \frac{c}{(n^*)^2 2^{2n_r+1}} \sum_{g=0}^{G(p)} \frac{\Gamma(2n_r - 2g + 1) (2g)!}{\Gamma(n_r - g + 1) \{g!\}^2 \Gamma(\alpha^* + n_r - g + 1)} \\
 &\quad \times \frac{\Gamma(2n_r - 2g + 2\alpha^* + 1) 2^{2n_r-p}}{(p-2g)! \Gamma(2\alpha^* + 2n_r - p + 1) \Gamma(2n_r - p + 1)}, \\
 I_p(q) &= \frac{\sqrt{\pi}}{2^{q+1}} \xi^q \Gamma(2n - p + q + 1) {}_2\tilde{F}_1 \left(\frac{1}{2}(2n - p + q + 1), \frac{1}{2}(2n - p + q + 2); q + \frac{3}{2}; -\xi^2 \right),
 \end{aligned}$$

where ${}_2\tilde{F}_1$ is the regularized hypergeometric function, and $\xi = kn$.

-
- [1] Hendrik Weimer, Markus Müller, Igor Lesanovsky, Peter Zoller and Hans Peter Büchler, *Nature Physics* **6**, 382 (2010)
- [2] I. Bloch, J. Dalibard, and S. Nascimbène, *Nature Physics* **8**, 267 (2012)
- [3] M. Saffman, T. Walker, and K. Molmer, *Rev. Mod. Phys.* **82**, 2313 (2010)
- [4] D. Jaksch, J. I. Cirac, P. Zoller, S. L. Rolston, R. Côté, and M. D. Lukin, *Phys. Rev. Lett.* **85**, 2208 (2000)
- [5] S. K. Dutta, J. R. Guest, D. Feldbaum, A. Walz-Flannighan, and Georg Riathel, *Phys. Rev. Lett.* **85**, 5551 (2000)
- [6] M. Saffman and T. G. Walker, *Phys. Rev. A* **72**, 022347 (2005)
- [7] K. C. Younge, S. E. Anderson and Georg Raithel, *New J. Phys.* **12**, 023031 (2010)
- [8] S. E. Anderson, K. C. Younge, and Georg Raithel, *Phys. Rev. Lett.* **107**, 263001 (2011)
- [9] S. Zhang, F. Robicheaux, and M. Saffman, *Phys. Rev. A* **84**, 043408 (2011)
- [10] J. Mosley, P. Hyafil, G. Nogues, M. Brune, J.-M. Raimond, and S. Haroche, *Eur. Phys. J. D* **35**, 43 (2005)
- [11] M. Mayle, I. Lesanovsky, and P. Schmelcher, *Phys. Rev. A* **79**, 041403(R) (2009)
- [12] L. J. LeBlanc and J. H. Thywissen, *Phys. Rev. A* **75**, 053612 (2007)
- [13] B. Arora, M. S. Safronova, and C. W. Clark, *Phys. Rev. A* **84**, 043401 (2011)
- [14] A. J. Daley, M. M. Boyd, J. Ye, and P. Zoller, *Phys. Rev. A* **101**, 170504 (2008)
- [15] M. Gajdacz, T. Opatrny, and K. K. Das, *Phys. Rev. A* **83**, 033623 (2011)
- [16] D. C. McKay and B. DeMarco, *Rep. Prog. Phys.* **74**, 054401 (2011)
- [17] K. C. Younge, B. Knuffman, S. E. Anderson, and G. Raithel, *Phys. Rev. Lett.* **104**, 173001 (2010)
- [18] T. Topcu and A. Derevianko, arXiv:**1305.6570** [physics.atom-ph] (2013)
- [19] T. Topcu and A. Derevianko, arXiv:**1308.0573** [physics.atom-ph] (2013)
- [20] T. F. Gallagher, *Rydberg Atoms* (Cambridge University Press, Cambridge, 2005)
- [21] S. E. Anderson and G. Raithel, *Phys. Rev. Lett.* **109**, 23001 (2012)
- [22] M. Greiner, O. Mandel, T. Esslinger, T. W. Hänsch, and I. Bloch, *Nat.* **415**, 39 (2002)
- [23] D. A. Varshalovich, A. N. Moskalev, and V. K. Khersonskii, *Quantum Theory of Angular Momentum* (World Scientific, 1989)
- [24] W. N. Bailey, *Q J Math* **os-10**, 60 (1939)
- [25] V. A. Kostelecky and M. M. Nieto, *Phys. Rev. A* **32**, 3243 (1985)